

Properties of filaments in solar cycle 20-23 from McIntosh Archive

Rakesh Mazumder

Center of Excellence in Space Sciences India, Indian Institute of Science Education and Research Kolkata, Mohanpur 741246, West Bengal, India; rm13rs027@iiserkol.ac.in

Received 2018 October 18; accepted 2018 November 29

Abstract A filament is a cool, dense structure suspended in the solar corona. The eruption of a filament is often associated with a coronal mass ejection (CME), which has an adverse effect on space weather. Hence, research on filaments has attracted much attention in the recent past. The tilt angle of active region (AR) magnetic bipoles is a crucial parameter in the context of the solar dynamo, which governs the conversion efficiency of the toroidal magnetic field to poloidal magnetic field. Filaments always form over polarity inversion lines (PILs), so the study of tilt angles for these filaments can provide valuable information about generation of a magnetic field in the Sun. We investigate the tilt angles of filaments and other properties using McIntosh Archive data. We fit a straight line to each filament to estimate its tilt angle. We examine the variation of mean tilt angle with time. The latitude distribution of positive tilt angle filaments and negative tilt angle filaments reveals that there is a dominance of positive tilt angle filaments in the southern hemisphere and negative tilt angle filaments dominate in the northern hemisphere. We study the variation of the mean tilt angle for low and high latitudes separately. Investigations of temporal variation with filament number indicate that total filament number and low latitude filament number vary cyclically, in phase with the solar cycle. There are fewer filaments at high latitudes and they also show a cyclic pattern in temporal variation. We also study the north-south asymmetry of filaments with different latitude criteria.

Key words: Sun: filaments, prominences — Sun: magnetic fields — Sun: corona — Sun: activity — (Sun:) sunspots

1 INTRODUCTION

Filaments are cool and dense structures that are suspended in the solar corona. They appear as dark filamentary structures when seen on the disk of the Sun. The same features appear bright when observed in the off-limb region, and are known as prominences for historical reasons. A filament always appears in the vicinity of polarity inversion lines (PILs) (also known as neutral lines) (Martin 1998). Filament eruption is often associated with a coronal mass ejection (CME), which is hazardous for space weather. Hence, the study of filament activity is important from the perspective of space weather research (Gopalswamy et al. 2003; Gilbert et al. 2000; Jing et al. 2004). Filaments are primarily observed in the $H\alpha$ line. Systematic $H\alpha$ observations have continued since 1915 at Kodaikanal Observatory (India), 1919 at Meudon Observatory (France) (spectroscopic observa-

tions) and 1959 at Kislovodsk Mountain Astronomical Station of the Main (Pulkovo) Astronomical Observatory of Russian Academy of Sciences. Tlatov et al. (2016) scrutinized data on filaments from more than eight solar cycles using synoptic maps from Meudon Observatory and Kislovodsk Mountain Station. Chatterjee et al. (2017) studied filament properties using Kodaikanal Observatory (India) data for nine solar cycles. Hao et al. (2015) investigated properties of filaments using data from Big Bear Solar Observatory (BBSO) from 1988 to 2013 and Mazumder et al. (2018) examined properties of filaments using McIntosh Archive data from 1967 to 2009.

Filaments are distributed uniformly in longitude (Mazumder et al. 2018). However, the distribution of filaments in latitude is not uniform. A bimodal nature in the latitudinal distribution of filaments has been observed (Hao et al. 2015; Mazumder et al. 2018). Tlatov et al. (2016), Chatterjee et al. (2017), Hao et al. (2015) and Mazumder

et al. (2018) reported a butterfly structure in the temporal variation of the latitudinal distribution of filaments. The butterfly diagram is similar to that of sunspots except that the spread in latitude is broader in the case of filaments. They also reported the rush to the pole of filaments during maxima in the solar cycle. The variation of filament number is found to be cyclic in close proximity to sunspot number variation (Hao et al. 2015; Li et al. 2010). The total filament length in the Carrington map is also found to vary cyclically with time (Tlatov et al. 2016; Mazumder et al. 2018). Mazumder et al. (2018) further classified filaments as associated or unassociated with solar activity belt according to their position inside or outside the sunspot activity belt respectively. They found the variation in total length of the filaments is correlated with variation in sunspot area. However, the temporal variation of length of filaments unassociated with solar activity belt is uncorrelated with variation of sunspot area.

The tilt angle of an active region (AR) is a crucial parameter in describing the solar dynamo. The tilt angle of AR magnetic bipoles governs the conversion efficiency of the toroidal magnetic field to poloidal magnetic field (Tlatov et al. 2013). Filaments always form over PILs, so the analysis of the tilt angle of filaments can give us important insights into the mechanism, generating the magnetic field of the Sun. The average tilt angle of filaments is found to decrease from the equator towards the pole for both positive and negative tilts (Tlatov et al. 2016; Mazumder et al. 2018), which is consistent with the famous Joy’s Law of sunspot pairs (Hale et al. 1919). The tilt angle of filament was observed to be negative in the northern hemisphere and positive in the southern hemisphere for different lengths and sunspot belt association criteria by Mazumder et al. (2018). Following this observation, they concluded that the origin of most filaments is from large-scale magnetic field structure and not from the AR. However, the geometry of an inter-AR filament as depicted by Martens & Zwaan (2001) can also contribute to this apparently unexpected tilt angle orientation in both hemispheres. The hemispheric asymmetry of the filament number was studied, and they were found to be asymmetric at different phases in the solar cycle (Mazumder et al. 2018; Hao et al. 2015; Kong et al. 2015; Li et al. 2010, 2003).

The mean tilt angle variation with time is observed to follow a solar cycle like variation (Tlatov et al. 2016). The latitudinal distribution of positive and negative tilt angles of filaments is observed to behave differently (Tlatov et al. 2016). The time latitude distribution of the filaments’ tilt

angle shows a positive tilt dominance in mid-latitude and a negative tilt dominance at higher latitude (Tlatov et al. 2016).

We have organized this paper as follows. In Section 2, we describe the data used and discuss the methods implemented to analyze the data. In Section 3, we analyze the results obtained. In Section 4, we summarize our work.

2 DATA AND METHODS

Patrick S. McIntosh, a scientist at NOAA’s Space Environment Center in Boulder, drew Carrington maps of the Sun using various ground- and space-based satellite data from April 1967 till July 2009. The hand-drawn maps were archived and digitized by the McIntosh project (a Boston College/NOAA/NCAR collaboration, funded by the NSF) at NOAA/NCEI. The data are stored in both image and FITS format and also have been made available online¹. For our analysis, we have used Level 3 FITS files from the McIntosh Archive (Gibson et al. 2017; Webb et al. 2017).

The Level 3 image of Carrington rotation number 1916 is presented in Figure 1. The Carrington maps contain spatial information of various solar features, namely sunspots, plages, filaments, coronal holes and PILs. In this work, we have studied different properties of filaments. There are three big gaps in the data: the first is from June 1974 to July 1978, the second from October 1991 to January 1994 and the final from April 1994 to May 1996. We have reduced the Level 3 FITS files using Interactive Data Language (IDL) and obtained spatial information on various solar features, namely: sunspots, plages, filaments, coronal holes and PILs. In this study, we are only interested in filaments, so we produce Carrington maps that contain only filaments. In total there are 442 Carrington maps available during April 1967 to July 2009, and we have detected 67 373 filaments. We fit a straight line to each filament. The angle that the straight line makes with the equator is defined as the tilt angle of that particular filament. One sample image of Carrington map 1552 containing only the filaments with the fitted straight lines is shown in Figure 2. The filaments are represented by green lines and the fitted straight lines are represented by red lines. We observe that the fittings are good except for a few cases which can be ignored in the statistical analysis. We calculate filament lengths using the following formula

$$L = \sum_n \sqrt{R_{\odot}^2 \delta\theta^2 + R_{\odot}^2 \cos^2 \theta \delta\phi^2}, \quad (1)$$

¹ <https://www2.hao.ucar.edu/mcIntosh-archive/four-cycles-solar-synoptic-maps>

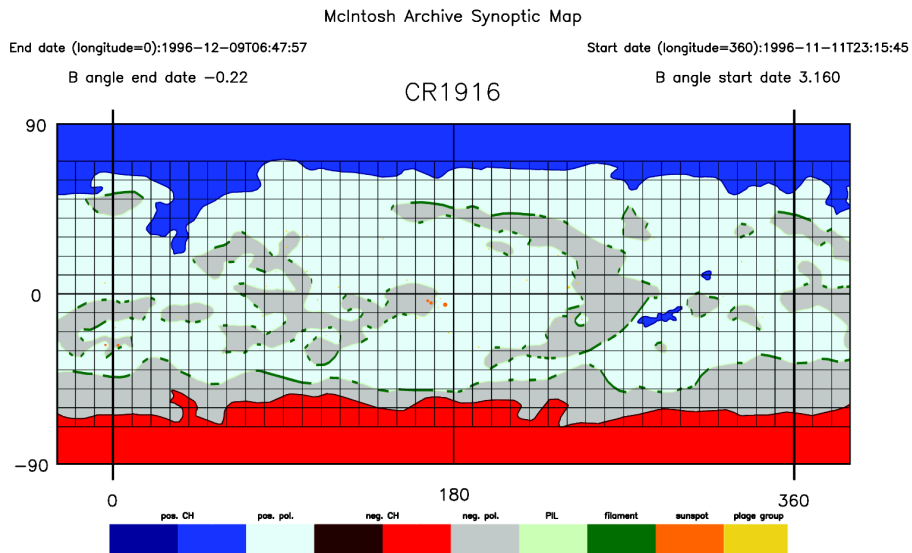


Fig. 1 Level 3 image of Carrington rotation number 1916 from the McIntosh Archive. Here, *gray* and *light blue patches* represent the negative and positive polarity magnetic fields respectively. The *red* and *dark blue patches* signify the negative and positive coronal holes respectively. *Dark green* and *light green lines* trace the filaments and PILs respectively.

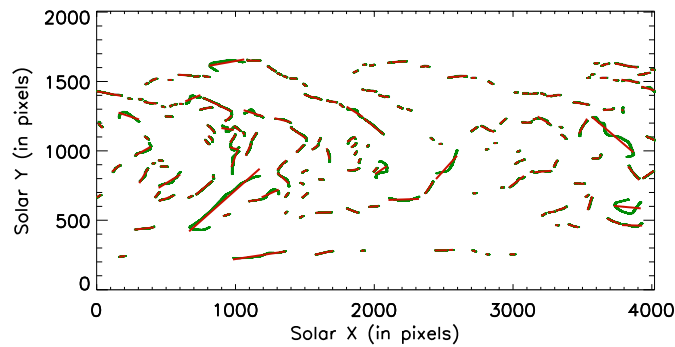


Fig. 2 Fitting of filaments by straight lines in a sample Carrington map (Carrington number 1552). The *green lines* represent filaments. The *red lines* indicate fitted straight lines.

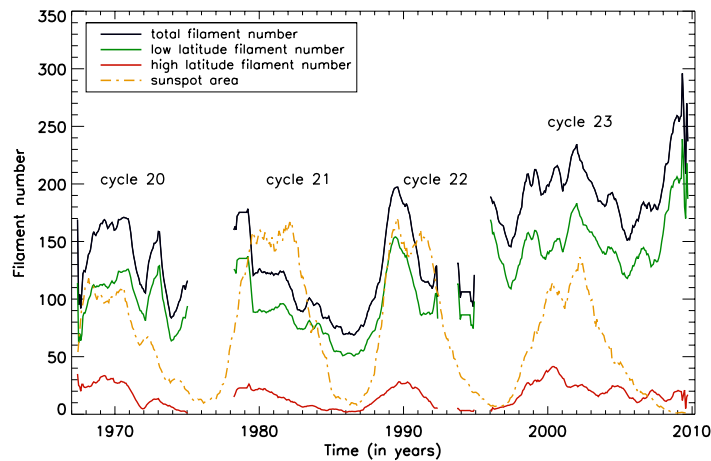


Fig. 3 Filament number variation with time. The *black line* shows the variation in total number of filaments with time. The *green line* depicts the variation of low latitude filament number with time. The *red line* represents the variation of high latitude filament number with time. The sunspot area variation is traced by the *orange dash-dotted line*.

where L is a filament's length, R_{\odot} is the solar radius, the symbols θ and ϕ mean the latitude and longitude of a particular pixel respectively, and n is the total number of pixels associated with a filament's structure. The quantities $\delta\theta$ and $\delta\phi$ are latitudinal and longitudinal differences between two adjacent pixels, respectively. We add the lengths of all the filaments in a Carrington map to get the total length of the all filaments in it. The sunspot data are taken from the Royal Greenwich Observatory (RGO) and US Air Force (USAF) - Solar Optical Observing Network (SOON) database.

3 ANALYSIS AND RESULTS

Filaments always appear in the vicinity of PILs (Martin 1998). Filament formation is closely related to generation of the magnetic field in the Sun. Figure 3 displays the variation of filament number with time. The black line shows the variation of total filament number with time. The green line depicts the variation of low latitude filament number with time. The red line represents the variation of high latitude filament number with time. The variation of sunspot area is signified by the orange dash-dotted line. We notice a cyclic variation of the total filament number and low latitude filament number which are in phase with the sunspot area variation. Although there are fewer high latitude filaments, they also show a cyclic variation (Li et al. 2007).

The tilt angle of an AR is a crucial parameter describing the solar dynamo. The tilt angle of AR magnetic bipoles governs the conversion efficiency of the toroidal magnetic field to poloidal magnetic field (Tlatov et al. 2013). Filaments always form over PILs. Thus, analysis of the tilt angle of filaments can give us important insights into the magnetic field generation mechanism inside the Sun. Here, we carry out a detailed analysis of the filaments' tilt angles.

Figure 4 presents the histogram of filament tilt angles. Out of a total 67 373 filaments, 33 415 filaments have positive tilt angle and 33 622 filaments have negative tilt angle. Consequently, in our database, there are 207 more filaments which have a negative tilt angle, when compared to filaments which have positive tilt angle.

Figure 5 shows the latitudinal distribution of positive tilt angle filaments. Out of a total 33 415 positive tilt angle filaments, 12 113 filaments are in the northern hemisphere and 21 297 filaments are in the southern hemisphere. Figure 6 exhibits the latitudinal distribution of negative tilt angle. Out of 33 622 total negative tilt angle fil-

aments, 20 305 filaments are in the northern hemisphere, and 13 315 filaments are in the southern hemisphere. So there exists a dominance of negative tilt angle in the northern hemisphere while a positive tilt angle dominates in the southern hemisphere. The findings are consistent with earlier findings by Mazumder et al. (2018).

Figure 7 depicts the variation of mean tilt angle with time. We calculate the mean of all of the tilt angles present in a particular Carrington map and derive the mean tilt angle. The black curve in Figure 7 represents the variation of the mean tilt angle with time. The red line depicts the temporal variation of the mean tilt angle averaged over 13 Carrington rotations. We further calculate the average tilt angle in each solar cycle. The green crosses signify solar cycle average mean tilt angle. In addition, we investigate the mean tilt angle for lower latitude and higher latitude filaments separately. We define lower latitude filaments to be filaments situated within latitude $\pm 40^\circ$ ($|\theta| < 40^\circ$) and we define higher latitude filaments as filaments having latitude either greater than 50° or filaments having latitude less than -50° ($|\theta| > 50^\circ$). The total number of low latitude filaments is 51 210, and the total number of high latitude filaments is 7564.

Figure 8 depicts the variation of low latitude mean tilt angle with time. The black line illustrates the low latitude mean tilt angle variation with time. The red line signifies the temporal variation of low latitude tilt angle averaged over 13 Carrington rotations. The green crosses mark solar cycle average mean tilt angle at low latitude.

Figure 9 depicts the variation of high latitude mean tilt angle with time. The black line traces high latitude mean tilt angle variation with time. The red line indicates the temporal variation of high latitude tilt angle averaged over 13 Carrington rotations. The green crosses signify solar cycle average mean tilt angle in high latitude.

Filament formation is not symmetric in the two hemispheres of the Sun. Earlier studies reported the north-south asymmetry of filament number (Hao et al. 2015; Kong et al. 2015; Li et al. 2010, 2003), but we believe that total filament length captures information about the magnetic field generation in the Sun better than the filament number (Mazumder et al. 2018). So, we use the total filament length in each Carrington rotation to calculate the north-south asymmetry of the filament. We define north-south asymmetry of sunspot area A_{sp} as

$$A_{sp} = \frac{N_{sp} - S_{sp}}{N_{sp} + S_{sp}}, \quad (2)$$

where N_{sp} and S_{sp} are the total area of the sunspots in the northern and southern hemispheres, respectively. If

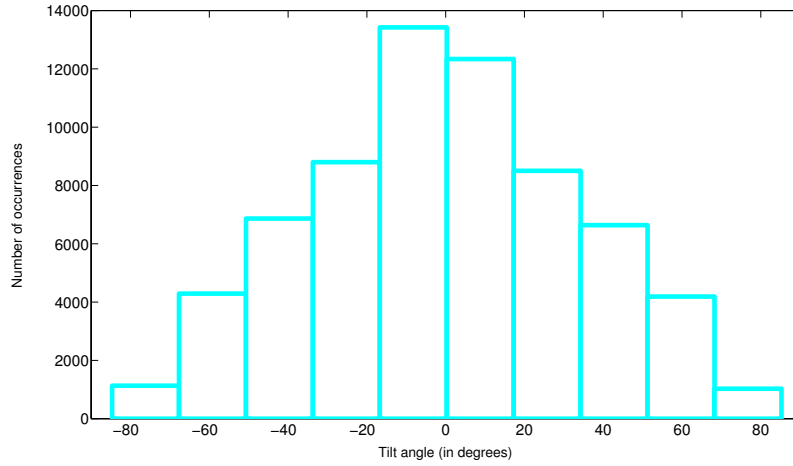


Fig. 4 Histogram of the tilt angle of filaments. There is an excess of negative tilt angle compared to positive tilt angle.

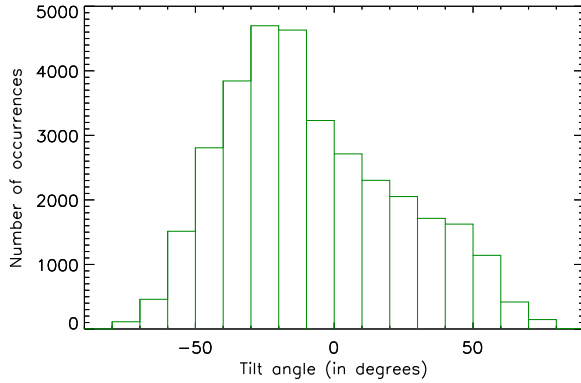


Fig. 5 Histogram of latitude of filaments having positive tilt angle. The southern hemisphere has more positive tilt angle filaments than the northern hemisphere.

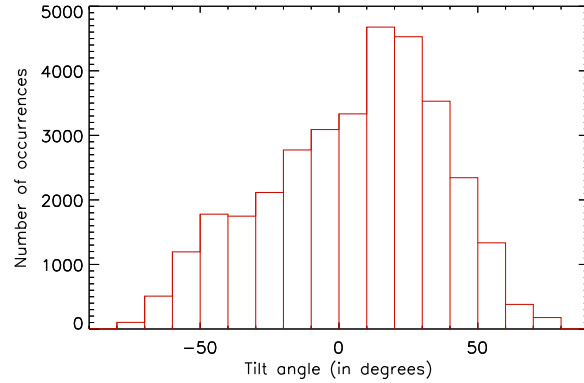


Fig. 6 Histogram of the latitude of filaments having negative tilt angle. The northern hemisphere has more negative tilt angle filaments than the southern hemisphere.

$A_{sp} > 0$, the total sunspot area in the northern hemisphere dominates over that in the southern hemisphere and if $A_{sp} < 0$, the total sunspot area in the southern hemisphere dominates over that in the northern hemisphere. We define north-south asymmetry of the filament (A_{fil}) as

$$A_{fil} = \frac{N_{fil} - S_{fil}}{N_{fil} + S_{fil}}, \quad (3)$$

where N_{fil} and S_{fil} are the total filament lengths in the northern and southern hemispheres, respectively. If $A_{fil} > 0$, the total filament length in the northern hemisphere dominates over that in the southern hemisphere and if $A_{fil} < 0$, the total filament length in the southern hemisphere dominates over that in the northern hemisphere.

Figure 10 depicts north-south asymmetry of the filament length and sunspot area for different latitude criteria. The blue crosses represent the north-south asymmetry of all filaments. The green crosses signify the north-south asymmetry of low latitude filaments. The red crosses

indicate the north-south asymmetry of high latitude filaments. The north-south asymmetry of sunspot area is shown by filled orange circles. The temporal variation of north-south asymmetry in all the filaments and low latitude filaments show a sunspot area north-south asymmetry like behavior. The north-south asymmetry of high latitude filaments fluctuates and does not show any correspondence with north-south asymmetry of sunspot area. However, the north-south asymmetry of the high latitude filaments exhibits dominance in the northern hemisphere during solar cycle 20, whereas in solar cycles 21, 22 and 23, the southern hemisphere manifests a dominant character (Li et al. 2009).

4 SUMMARY AND CONCLUSIONS

We have analyzed 442 Carrington maps from the McIntosh database and detected 67 373 filaments. Each filament is fitted with a straight line, and the tilt angle (angle which

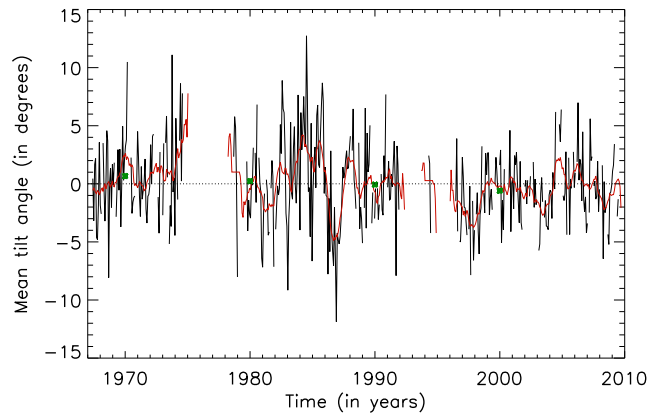


Fig. 7 Mean tilt angle variation with time. The black line shows the time variation of the mean tilt angle. The red line depicts temporal variation of the mean tilt angle averaged over 13 Carrington rotations. The green crosses represent solar cycle average mean tilt angle.

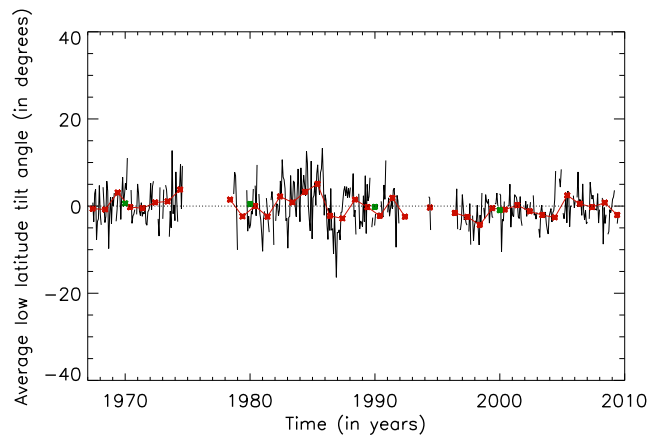


Fig. 8 Mean tilt angle variation of low latitude filament with time. The black line depicts the low latitude mean tilt angle variation with time. The red line shows the temporal variation of low latitude mean tilt angle averaged over 13 Carrington rotations. The green crosses represent solar cycle average mean tilt angle.

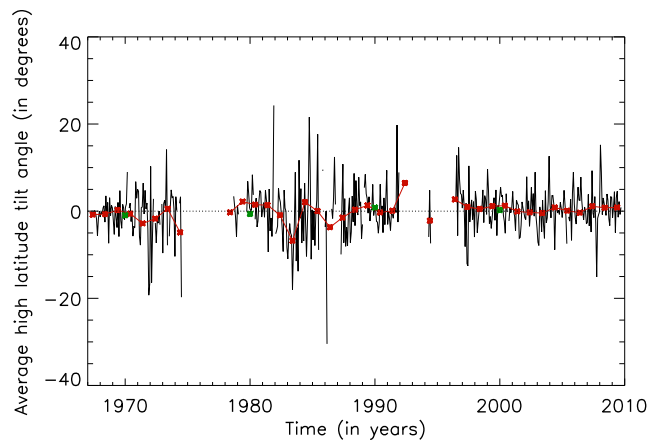


Fig. 9 Mean tilt angle variation of high latitude filament with time. The black line depicts the high latitude mean tilt angle variation with time. The red line shows the temporal variation of high latitude mean tilt angle averaged over 13 Carrington rotations. The green crosses represent solar cycle average mean tilt angle.

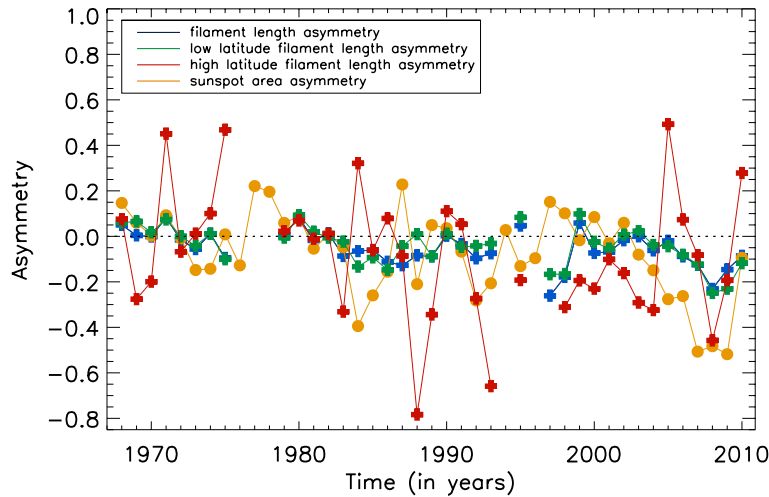


Fig. 10 Hemispheric asymmetry of filament and sunspot area. The *blue crosses* represent the north-south asymmetry of all filaments. The *green crosses* indicate the north-south asymmetry of low latitude filaments. The *red crosses* signify the north-south asymmetry of high latitude filaments. The north-south asymmetry of sunspot area is depicted by *filled orange circles*.

the straight line makes with equator) is estimated. We have noticed a cyclic variation of the total filament number as well as in low latitude and high latitude filament numbers (see Fig. 3). A detailed analysis of tilt angles of the filaments is carried out in this work. Figure 2 shows an example of fitting of the filaments (depicted by green lines) with the straight lines (depicted by red straight lines) for Carrington map 1552. The histogram of tilt angle of all filaments is plotted (see Fig. 4), and we have found an excess of 207 negative tilt angle filaments as compared to the positive tilt angle filaments. The histogram of latitude for positive tilt angle filament reveals that positive tilt angle is dominant in the southern hemisphere (see Fig. 5). The histogram of latitude for negative tilt angle filaments demonstrates that negative tilt angle is dominant in the northern hemisphere (see Fig. 6). These findings are consistent with an earlier report (Mazumder et al. 2018) and contradict our expectation of positive tilt angle dominance in the northern hemisphere and negative tilt angle dominance in the southern hemisphere according to Hale’s polarity law in the two hemispheres (Hale et al. 1919). This can happen due to the contribution of inter-AR filament formation geometry as explained by Martens & Zwaan (2001). Another possible explanation is that more filaments are formed from large-scale magnetic field structure than from the intra-AR filament (Mazumder et al. 2018). We examined the variation of the mean tilt angle (mean of the tilt angle of all filaments in a Carrington map) and cycle-averaged tilt angle (see Fig. 7). We also studied mean tilt angle variation in low latitude ($|\theta| < 40^\circ$) and high latitude ($|\theta| > 50^\circ$) (see Fig. 8 and Fig. 9). Similar analysis carried out by Tlatov

et al. (2016) (from a different database) had more extended and continuous data. Consequently, we are skeptical about comparing our results to their findings. The north-south asymmetry of all the filaments, low latitude filaments and high latitude filaments points to a sunspot area north-south asymmetry like behavior in the case of all filaments and low latitude filaments (see Fig. 10). The north-south asymmetry of high latitude filaments fluctuates and does not show any correspondence with sunspot area north-south asymmetry. However, the north-south asymmetry of high latitude filaments exhibits a dominance of northern hemisphere in solar cycle 20 whereas in the solar cycles 21, 22 and 23 the southern hemisphere manifests a dominant character (Li et al. 2009).

Acknowledgements We are thankful to Patrick S. McIntosh, from NOAA’s Space Environment Center in Boulder, for developing the archive of hand-drawn Carrington maps using both ground-based and satellite observations. We are also grateful to the team at the McIntosh Archive project (a Boston College/NOAA/NCAR collaboration, funded by the NSF), based at NOAA National Centers for Environmental Information, for creating a digital archive of McIntosh Carrington maps and making it available online. R.M. acknowledges the grant from the University Grant Commission, Government of India and CESSI, IISER Kolkata, India.

References

Chatterjee, S., Hegde, M., Banerjee, D., & Ravindra, B. 2017, *ApJ*, 849, 44

- Gibson, S. E., Webb, D., Hewins, I. M., et al. 2017, in IAU Symposium, 328, *Living Around Active Stars*, eds. D. Nandy, A. Valio, & P. Petit, 93
- Gilbert, H. R., Holzer, T. E., Burkepile, J. T., & Hundhausen, A. J. 2000, *ApJ*, 537, 503
- Gopalswamy, N., Shimojo, M., Lu, W., et al. 2003, *ApJ*, 586, 562
- Hale, G. E., Ellerman, F., Nicholson, S. B., & Joy, A. H. 1919, *ApJ*, 49, 153
- Hao, Q., Fang, C., Cao, W., & Chen, P. F. 2015, *ApJS*, 221, 33
- Jing, J., Yurchyshyn, V. B., Yang, G., Xu, Y., & Wang, H. 2004, *ApJ*, 614, 1054
- Kong, D.-F., Qu, Z.-N., & Guo, Q.-L. 2015, *RAA (Research in Astronomy and Astrophysics)*, 15, 77
- Li, K. J., Gao, P. X., Zhan, L. S., Shi, X. J., & Zhu, W. W. 2009, *MNRAS*, 394, 231
- Li, K. J., Liu, X. H., Gao, P. X., & Zhan, L. S. 2010, *New Astron.*, 15, 346
- Li, K. J., Liu, X. H., Zhan, L. S., et al. 2003, *New Astron.*, 8, 655
- Li, K. J., Mu, J., & Li, Q. X. 2007, *MNRAS*, 376, L39
- Martens, P. C., & Zwaan, C. 2001, *ApJ*, 558, 872
- Martin, S. F. 1998, *Sol. Phys.*, 182, 107
- Mazumder, R., Bhowmik, P., & Nandy, D. 2018, *ApJ*, 868, 52
- Tlatov, A. G., Kuzanyan, K. M., & Vasil'yeva, V. V. 2016, *Sol. Phys.*, 291, 1115
- Tlatov, A., Illarionov, E., Sokoloff, D., & Pipin, V. 2013, *MNRAS*, 432, 2975
- Webb, D. F., Gibson, S. E., Hewins, I. M., et al. 2017, *Space Weather*, 15, 1442